remote sensing

MDPI

Technical Note

Radiological Assessment on Interest Areas on the Sellafield Nuclear Site via Unmanned Aerial Vehicle

Peter G. Martin [1,*], James Moore [2], John S. Fardoulis [1], Oliver D. Payton [1] and Thomas B. Scott [1]

[1] Interface Analysis Centre, School of Physics, HH Wills Physics Laboratory, University of Bristol, Tyndall Avenue, Bristol BS8 1TL, UK; john.fardoulis@bristol.ac.uk (J.S.F.); oliver.payton@bristol.ac.uk (O.D.P.); t.b.scott@bristol.ac.uk (T.B.S.)

[2] Sellafield Ltd., Sellafield, Seascale, Cumbria CA20 1PG, UK; james.d.moore@sellafieldsites.com

* Correspondence: peter.martin@bristol.ac.uk; Tel.: +44-117-33-17684

Academic Editors: Richard Müller and Prasad S. Thenkabail

Received: 16 September 2016; Accepted: 28 October 2016; Published: 3 November 2016

Abstract: The Sellafield nuclear plant is a 3 km^2 site in north-west Cumbria, England, with a long and distinguished history of nuclear power generation, reprocessing and waste storage—with a current working emphasis on decommissioning and clean-up. Important to this safe, efficient and complete remediation of the site, routine monitoring is essential in a wide range of on-site environments and structures to attain: (i) accurately map the evolving distribution of radiation with the best possible accuracy (sensitivity and spatial resolution); in addition to (ii) the contributing radionuclide species and therefore the radiological and chemo-toxicity risk. This work presents the trial deployment of an unmanned aerial vehicle equipped with a lightweight radiation detection system as a novel tool for the assessment of radioactivity at a number of test-sites on the nuclear licenced site. Through the use of this system, it was possible to determine the existence of anthropogenically present radiation at selected facilities. Such a system has been proven to be highly accurate (spatially) and precise (attribution of contamination species observed) within the challenging site environments, capable of measuring and mapping contamination over both high and low dose-rate areas.

Keywords: Sellafield; contamination; nuclear waste; reprocessing; radiation; UAV; mapping; sensor-fusion

1. Introduction

From its initial activities in the 1950s amidst the Cold War, with the construction of the Windscale Piles in order to produce material for the UK's nuclear weapons, Sellafield has represented the central location for the country's nuclear program, for energy generation and early military applications. Since the initial construction on farmland on the West-Cumbrian coast, the site now comprises a total of seven decommissioned reactors, centralised storage for the UK's high-level nuclear wastes (until a long-term disposal plan can be finalised), considerable reprocessing operations as well as hundreds of other buildings associated with radioactive material handling, many of which have since been demolished down to ground-level. The site also contains a large number of administrative buildings associated with the wide-range of ongoing site restoration activities.

As part of the long-term restorative plan for the site, there exists the target for all operations to have been completed by the year 2120. With this, an extensive programme of decommissioning and post-operational clean-out (POCO) is underway. This restoration has been estimated to cost in excess of £80 billion [1] and will require the next 100 years to complete. Forming a major part of this decommissioning, buildings that once existing as a central part of operations on-site are having to be demolished—with the target of no residual radiological trace of their presence. Hence, the radiological assay of these former buildings and eventually the sites on which they existed, for any possible traces of radioactive contamination, is important in the final declassification and withdrawal process.

The majority of the site will now be moving into a decommissioning and dismantling phase, with some active operations still continuing as part of ongoing reprocessing work on existing fuels, waste effluent treatment and storage prior to its long-term disposal within the UK. As there is no geological disposal facility (GDF) in the UK, the Sellafield site provides secure interim storage of this material until such a time it can be finally emplaced into a national GDF. On-going waste processing and storage activities necessitate the continual and highly spatially accurate monitoring of radiation across the site in order to detect any increases in radioactivity above those normally experienced within certain "active" areas.

A wide range of techniques are employed across the site with monitoring conducted using a combination of handheld mobile survey monitors and strategically positioned static monitoring points. Due to the age of the Sellafield site, and the way by which it evolved rapidly over its lifespan as a result of the ever-changing roles and demands placed upon it, nearly all of the mobile monitoring work performed around the site is conducted by people carrying mobile detection systems. Whilst representing a simple means by which to obtain a large volume of data, important to the safe stewardship of the site, such measurement methods incur a level of dose uptake to the operator. Further complications arise with the deployment of people to measure and monitor radiation due to difficulties in accessing certain locations/positions. Having been constructed without a view to their eventual decommissioning, certain structures and facilities may present significant access issues and hence high-quality measurements would be unachievable. The routine monitoring and inspection of places such as the roofs of buildings, high external walls and other positions at height pose their own challenges.

Through the deployment of an autonomous unmanned aerial vehicle (UAV) the levels of radioactivity within an area may be monitored with high spatial and spectral accuracy and with reduced human risk. When using a micro gamma-spectrometer it is possible to provide an "isotopic fingerprint" of the contributing contaminant species present, providing improved characterisation of radiological risk. Other advantages include a time, date and position fixed data to allow for time separated studies.

Previous airborne studies to examine the distribution of radiation within the environment have been conducted using heavy suitcase sized gamma-ray detectors (carried by fixed-wing aircraft or large helicopter platforms) [2–5]; being applied to regional geophysical investigations [6] as well as the monitoring of contamination that resulted from the 2011 Fukushima accident [7,8].

2. Materials and Methods

2.1. Unmanned Aerial Vehicle

Following from earlier work by some of the authors [9], the unmanned aerial vehicle detailed schematically in Figure 1 (with an image of the system shown within [10] used during this study was designed and constructed in-house at the University of Bristol (UK), with system development and deployment in various settings detailed by Martin [10,11]. With total dimensions of 1.2 m from propeller tip to tip, a height of 0.4 m fully assembled and a total weight of 7.0 kg including the lithium polymer batteries, the UAV was capable of 30–35 min flight durations when fully charged. The maximum payload capacity of the instrument is 5.0 kg, but to allow for the greatest possible flight durations for mapping, the integrated radiation mapping payload had a total mass of 0.5 kg. For ease of both storage and transportation, the entire UAV system could be rapidly disassembled and stored within a conventional large suitcase-sized box. Through the use of eight motors and propellers, mounted above and below the arms, a redundancy in operation was achieved should any one (or multiple) fail during flight.

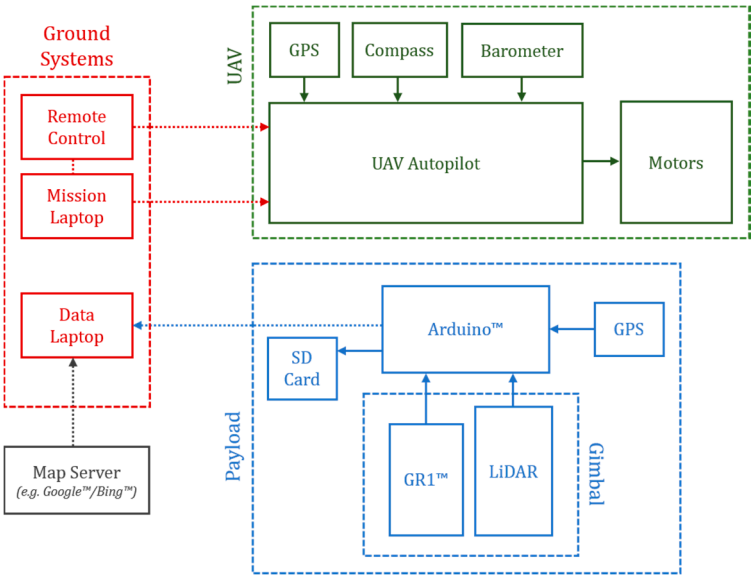

Figure 1. Schematic of the unmanned aerial vehicle (UAV), associated ground-based systems and radiation detection payload used within the contamination mapping works on the site.

Both take-off and landing of the UAV were conducted using conventional radio-based remote controls, with inflight control being performed using the open-source Arduino™ based Arducopter APM (Ardu-Pilot Mega) platform [12]. Controlled via the associated Mission Planner™ software; the UAV conducted radiation mapping autonomously using a series of predetermined aerial waypoints and altitudes. To provide high spatial accuracy during its operation, the UAV contained an on-board high-frequency (10 Hz update) GPS unit (Adafruit Ultimate GPS Breakout (New York, NY, USA) (MTK3339 Ver. 3.0 chip)) alongside a barometric pressure sensor for altitude. A miniature camera mounted on the front of the unit provided live video streaming back to the operator to assist with piloting the UAV.

2.2. Detection and Measurement

The lightweight (0.5 kg) radiation mapping payload used within this study featured a miniature gamma-ray spectrometer, produced by Kromek™. The uncollimated small volume (1 cm^3) cadmium zinc telluride (CZT) co-planar grid spectrometer has an energy range of 30 keV to 3.0 MeV, with an energy resolution of <2.5% @ 662 keV. Electrical noise within the detector was <10 keV Full Width at Half Maximum (FWHM) [13].

During operation of the UAV, measurements were taken at 500 ms (2 Hz) intervals. At each location, a high accuracy GPS (Adafruit Ultimate GPS Breakout (New York, NY, USA) (MTK3339 Ver. 3.0 chip)) position (±0.5 m) was coincidentally recorded (the prescribed accuracy attainable by typical GPS systems (undifferentiated) is approximately 1–3 m, however a greater accuracy was largely obtained during this work) in addition to a spectrum of the incoming incident radiation collected over the sampling period. A third incoming data stream recording height above the ground, was obtained from a high accuracy single-point laser rangefinder (AR2500 Acuity^{TM}) with an accuracy of ±5 cm over the 0.2 to 30 m instrumental range. All three incoming data streams were simultaneously collated onto an Arduino™ Mega ADK microcontroller contained within the payload system. The gamma-spectrometer and rangefinder, mounted side by side, were fixed onto a three-axis active gimballed stage in order to keep both instruments continuously pointing vertically at the ground surface—irrespective of the movements of the UAV whilst in the air. Operating at a wavelength of 905 nm, the rangefinder operates within the near infrared as a Class 1 eye-safe laser [14].

2.3. Data Acquisition

Data collection flights were carried out at a consistent ground equivalent speed of 1.5 ms^{-1}, with the instrument operated at the lowest height safe to do so (typically 1–10 m above the ground surface) taking into account obstructions such as trees, buildings and power distribution lines. A grid spacing of 2.0 m was maintained during the survey, conducted using a snaking "zig-zag" pattern to ensure full and efficient coverage of the survey area. A high-degree of positional accuracy achievable through the use of the GPS units utilized within this work allowed for a 2 m grid to be employed.

The study sites on the Sellafield site were chosen to represent challenges to the UAV system at two typical locations. One site (Loc. 1) comprised a number of large metallic containers, enclosed within a secure compound, where material was held before being sent off-site. The other study location (Loc. 2) represented a further storage area on site; a larger warehouse facility in which material was stored pending additional processing and treatment within the waste material cycle.

Whilst a 2 m grid spacing was selected for data acquisition within this work; predominantly as a result of the highly accurate GPS position achievable and small size of the areas to be surveyed, a much greater grid-spacing (as well as flight speed and altitude) would be employed for the radiation mapping of larger (km-scale) areas with the UAV.

2.4. Data Analysis

To interrogate the data acquired by the UAV system, custom analysis software was produced alongside existing software platforms. Maps of radiation intensity were plotted as color scaled heat maps detailing radiation levels (in counts per second (CPS)) overlain onto a base map. These maps incorporated counts measured from across the entire measurable energy range of the detector (30 keV to 3.0 MeV). The contour maps presented in this work were produced using LabVIEW™ 2016 (National Instruments, Austin, TX, USA) through the application of a nearest-neighbor smoothing algorithm within the software, by which the adjoining data-points are directly compared and averaging conducted (as appropriate).

At each of the measurement points—consisting of: (i) the GPS derived location of the device; (ii) the height above the ground of the system above ground from the single-point rangefinder; and (iii) a gamma-spectrum acquired over the collection period—a software normalisation was made to a height of 1 m. This normalisation was conducted with the possible source area of the contamination on the ground existing as a function of the horizontal aperture of the detector and its altitude, with the value produced following an inverse-square law calculation of radiation dispersion originating from a point source, with height produced by the laser rangefinder. The source of the radiation incident onto the detector does not originate solely from the infinitely small point directly below the detector, but from the region under the detector unit—visualized as circular in nature. With the continual rapid read-out from the detection system, where the circular plotted measurement points overlapped, an average of the coincident values detected was plotted. The use of the inverse-square scaling algorithm to correct measurements recorded at altitude back to 1 m above the surface follows on from earlier work by the authors [10,11], with measurements taken at altitude directly compared with those obtained at ground level using an identical detector setup (results not shown).

From the custom-built software, the outputted data consisted of longitude and latitude arrays as well as values for CPS and ground surface height (calculated from the difference between the GPS altitude and distance to the surface measured with the rangefinder). However, to allow for more sophisticated 3D plotting and visualization of the data onto surfaces, further software was produced in-house to convert this radiation data into the XML format (employed by commercial platforms). The complex nature of the site with many large high-sided buildings meant that GPS-derived values were occasionally erroneous due to signal reflection and coverage blackspots. With the software produced identifying and removing these points.

Unlike detection systems such as those featuring Geiger–Muller tubes or the more basic ionisation type sensors, the use of a light-weight gamma-ray spectrometer enables specific points on the site to

be isotopically resolved for their contributing contamination. Within the analysis software, specific regions of interest can be selected from the radiation map of a larger area—with the incident counts recorded at the different gamma-energies summed to yield a spectrum.

2.5. Detector Calibration

To allow for a conversion between the detector specific measurement of CPS (different for each detector—existing as a function of numerous intrinsic properties such as detector volume, type and any around detector shielding etc.) and the more applicable units of dose-rate (μSv/h) a series of calibrations were undertaken. To derive a dose-rate from CPS—a number of count-rate measurements (using the identical detector to the one used in the UAV study) from a number of different dose-rate and isotopic sources were obtained alongside measurements using a calibrated dosimeter from RADEX™ (Moscow, Russia). The dose-rate incident onto the detector is dependent on the energy of the individual gamma-rays, with the mass attenuation co-efficient (absorption) of gamma-ray photons described by the U.S. National Institute of Standards and Technology (NIST) [15]. A comparison of the measurements obtained from both detectors are shown in Figure A1. From this inter-detector comparison, a linear trend is observed to occur, with a count-rate of 500 CPS equating approximately to a dose-rate of 1 μSv/h. Due to the differing photon detection efficiencies that exist for the GR1 unit (and other radiation detectors)—a greater intrinsic efficiency for photon absorption at lower energies is encountered, with an exponential decline observed with higher incident photon energies. The software produced for this work negates this through the use of an increasing weighting factor with increasing gamma-ray energy (channel number). To derive a dose-rate from gamma-ray spectra, the analysis of the pulse-heights within the spectrum is typically undertaken. However, due to the complex and irregular nature of the gamma-ray spectra obtained, combined with the known energy dependence of the GR1 to differing gamma energies has led to the use of the count-rate being employed to estimate the dose-rate over the more favorable pulse-height method.

In order for the contributing gamma-ray peaks to be identified and attributed to specific radionuclides, a channel-number to photon energy calibration was undertaken (not shown). Using the GR1 detector unit; spectra of various radionuclides with well-defined emissions (^{137}Cs, ^{134}Cs, ^{60}Co, ^{110m}Ag, ^{129m}Te and ^{140}Ba) were recorded, with a calibration constant of 0.7553 keV/channel derived.

3. Results

The radiation map obtained from Loc. 1, the secure storage area containing the large metallic storage containers is shown within Figure 2. From the radiation intensity plot, the location of several of the large containers within the site (which itself presents no other radiological contamination) is clearly visible. Each of the containers shows an activity and dose-rate, corrected to a height of 1 m above the emitting surface, a number of times that of the background level of the tarmac surface surrounding the containers. A reference radiation level representing the background activity/dose-rate measured away from any radioactive material or contamination on the site is shown on the radiation intensity profile (A–B) on Figure 2, the exact radiation level recorded at each of the sites or the site background level cannot be disclosed due to the nature of the site.

The highly isolated nature of the radiation hotspot is evidenced by the transect representing the detected activity/radiation intensity along the line A–B. As would be anticipated, directly over the storage containers the radiation level is at its greatest, however, at a distance of approximately 5 m either side of this maximum value the intensity is observed to decrease by over 50%, with a distance of 12 m from this maximum—the level detected is equitable to typically observed background levels.

A classification of the material encased within the containers is produced via the gamma-ray spectra of the area in Loc. 1 (identified within Figure 2), is shown in Figure 3. From this gamma-ray spectrum, the presence of a number of different fission product isotopes is apparent. Such species include the short and medium-lived fission products; Europium (^{150}Eu and ^{154}Eu), Antimony (^{126}Sb), Ruthenium (^{106}Ru), Zirconium (^{95D}Zr), Niobium (^{95}Nb) and Tellurium (^{133m}Te), of which ^{95}Nb exists

as the daughter product following the radiogenic decay of its parent ^{95}Zr with a half-life of only 64 days [16], ^{95}Nb decays to the stable isotope to ^{95}Mo with a half-life of 34.99 days [16]. These species, as well as the other species detected, are all produced as by-products that accumulate through the typical irradiation of nuclear fuel within a reactor during standard fuel generation operations.

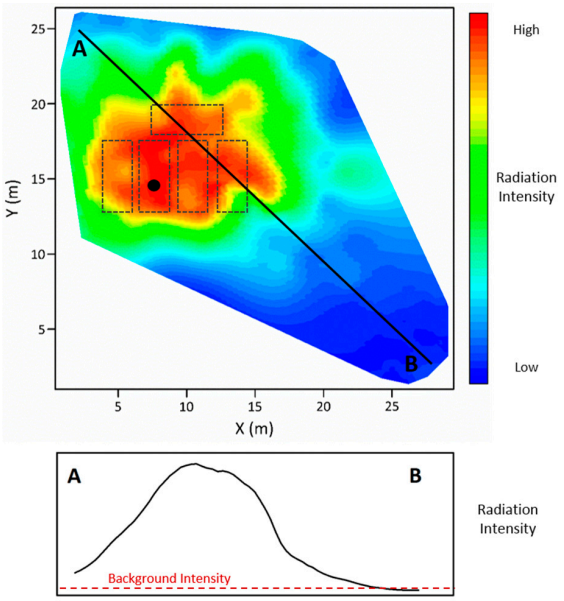

Figure 2. Radiation intensity map obtained by the UAV over the secure freight storage container compound (Loc. 1). An elevated radiation intensity is observed centred on the location of the five containers positioned within the area at the time of the survey. The location of the gamma-spectrum (Figure 3) is identified (●). From the transect line A–B, the sharp rise in detected radiation is apparent.

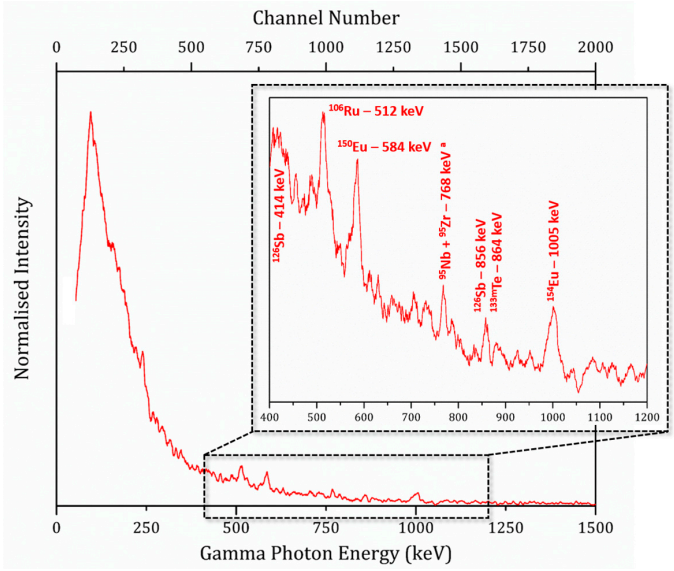

Figure 3. Gamma-ray spectra obtained over Loc. 1, the secure compound containing the five large shipping containers. The contributing radionuclide peaks and their corresponding energies are identified.

Similarly, the radiation map produced by the UAV over Loc. 2, the large interim-storage warehouse facility, is presented in Figure 4. The radiation map of Loc. 2 is similar to that of Loc. 1, with the location of the radioactive material being apparent in relation to the low-activity of its surroundings.

A radiation intensity profile (A–B) like that shown in Figure 2 is also presented, with the reference site background shown. With respect to the contamination (again normalised to a height of 1 meter above the emitting surface), the total radiation intensity level is less than that from Loc. 1, likely reflecting the volume of material and any shielding surrounding the active material stored in the facility. The gamma-ray spectrum for the point indicated at Loc. 2 is shown in Figure 5. Like the spectrum from Loc. 1, this spectra shows a number of characteristic peaks for a number of isotopic species that are present, however, as the material that exists at this storage facility is the result of different activities on the Sellafield site than at Loc. 1, different characteristic peaks are apparent. The two dominant peaks on this plot are the high-energy points corresponding to the radioisotope of Cobalt (^{60}Co; half-life of 5.27 years [16]) with its characteristic emissions at 1173 and 1330 keV. Discernible peaks for the common fission product isotopes of cesium (^{134}Cs and ^{137}Cs; half-lives of 2.065 and 30.17 years respectively [16]) are observed at the lower gamma-energies. The isotopes of cesium are produced in abundance during the typical operation of a nuclear reactor, from the fission (splitting) of the ^{235}U atoms present in the fuel.

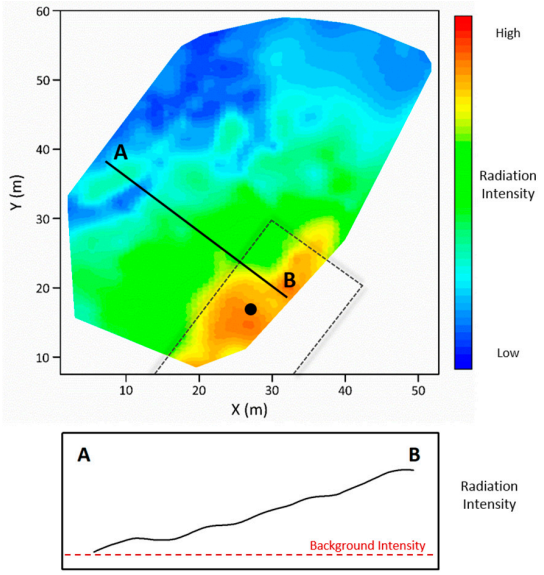

Figure 4. Radiation map obtained over by the UAV over the interim storage facility and the surrounding area (Loc. 2). The location of the corner of the large building is apparent by the marked increase in radiation intensity. The location of the gamma-spectrum (Figure 5) is identified (•). A similar transect (A–B) to Figure 2, (Loc. 1) here depicts a more gradual increase in the activity detected towards the centre of the storage building.

Because of the high radioactivity of both Cs and Co isotopes, their monitored and secure short-term interim storage prior to later processing steps is typically performed.

As would be anticipated from a site such as Sellafield, which possesses a range of radiological hazards within its confines, extreme care and attention have to be paid to ensure the safe storage and packaging of its wastes across the site and the dose that it would likely present to its staff and the wider public. The simplest means by which to limit the radiation received by those on the ground is the intelligent positioning of material. As such, emitted radiation is attenuated by the shielding and absorption provided by less active or denser materials. As personnel do not pass directly above waste stores, the level of radiation escaping directly upwards is greater than would be encountered out sideways due to stronger radiation "shine paths", where people could be moving, (ceilings of radiation stores are not shielded to the same extent as walls due to access requirements and weight limitations). As a result, the activity (and the hence the collected gamma-spectra) measured by the UAV would be more typical of the material housed within the stores. Due to the impact of considerable shielding that

exists sideways from the store, this at-altitude monitoring would allow for a better insight into the nature/state of the material otherwise possible.

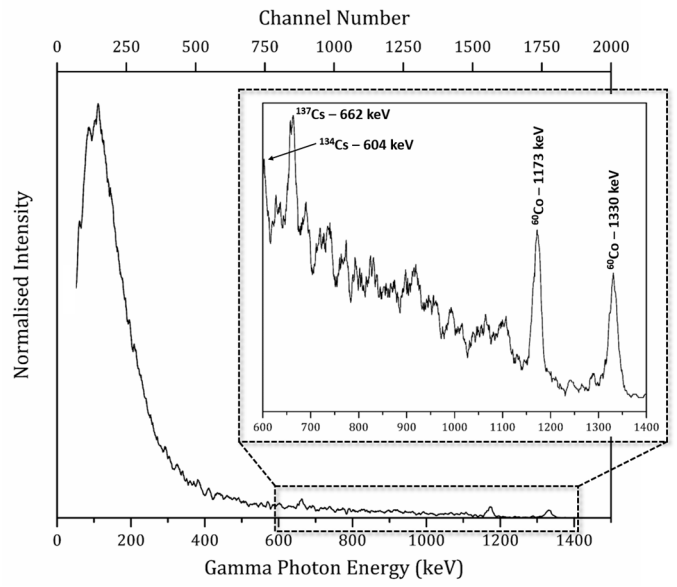

Figure 5. Gamma-ray spectra obtained over Loc. 2, the large warehouse style interim storage site housing material progressing through the reprocessing cycle. Unlike the spectra produced from Loc. 1 (Figure 3), there are fewer contributing radionuclide species.

4. Discussion

Through the application of a UAV to conduct radiation mapping on the Sellafield nuclear licenced site, the location and distribution of stored radioactive material and the contributing radionuclides were successfully identified on two test sites known to exhibit low levels of radiation. Using the UAV system, a level of spatial resolution not previously achievable was obtained and in locations where controlled access would otherwise be required due to the radiological hazard. Unlike with surveys performed by people, a UAV survey does not introduce the effects of shielding from the operator that would otherwise be encountered, and simultaneously reduces worker exposure to radiation. As the UAV platform is highly autonomous, this represents only a small need for trained staff to operate the system, with only take-off and landing requiring real-time piloting from the pilot. This high degree of automation (with the route of each survey saved as a collection of GPS waypoints, altitudes and velocities) permits the same survey to be repeatedly conducted to study any change in the distribution of radioactivity over time.

The real-time data collection and transmission through a secured network to a ground station not only allows the operators conducting the works to view the results as the survey progresses but also enables the near real-time integration and inclusion of the results into the site-wide monitoring system.

In line with UK CAA guidelines, the UAV weighs less than the 7.0 kg in order for the system to be classified as a small unmanned aircraft under article 166 [17]. This low total mass, coupled with the in-built redundancy of the aerial system through the use of eight rotor blades arranged in an above and below X8 configuration, has also satisfied the Sellafield site management that the system represents a low risk of structural damage to buildings during its operation. Safety considerations with respect to the high-speed at which the UAVs rotor blades spin and the potential for injury as a result, require personnel not actively involved in the survey to remain well clear of the area whilst the work is performed.

As well as examining the radiological contamination over an area, the vantage point offered by a surveying UAV can be useful for other aspects of site monitoring and assurance. The installation of a

range of cameras (e.g., conventional photo/video, hyperspectral and infra-red (IR)) on the underside of the platform, potentially co-incident with the radiation mapping system, would allow for structural issues or defects with the outer shell of a building to be determined. The inclusion of a single-point laser rangefinder within the payload for the normalisation of measured radioactivity to a height of 1 m above the ground, allows for a point-cloud DEM of each of the locations to be constructed through combining the additional data obtained by the on-board GPS unit (not shown within this work). This rendering would enable the generation of basic 3-dimensional radiation map of a site.

5. Conclusions

Proven to be effectual in the overhead monitoring of active materials on the Sellafield nuclear licensed site, the system as deployed—with its inherent stability in the air and the considerable flight time—has the potential for use in other applications beyond Sellafield, such as the detection of orphan material for potential homeland security scenarios. Furthermore, the ability of the UAV to be rapidly deployed; coupled with its in-air autonomy and simple operator input would allow this system to be employed as a powerful tool in the response to an on-site radiological incident where both rapid and large area coverage is required.

Acknowledgments: The authors wish to thank Sellafield Ltd. for their support of this work by allowing system testing to be conducted on active areas of their site. This work was funded by the University of Bristol EPSRC Impact Acceleration Fund (Grant Reference: EP/K503824/1), who fund the Open Access publication of this work. The University of Bristol Physics workshop must also be thanked for their technical assistance on the project.

Author Contributions: Oliver Payton and Tom Scott. conceived the idea for the platform; Oliver Payton produced the software for data collection; John Fardoulis designed the UAV, was pilot system pilot and responsible for flight operations and CAA clearance to operate in restricted airspace; all authors contributed to the on-site study; Peter Martin analysed the data obtained and produced the manuscript figures; Peter Martin produced the manuscript with assistance from James Moore, Tom Scott and Oliver Payton.

Conflicts of Interest: The authors declare no conflict of interest. The founding sponsors had no role in the design of the study; in the collection, analyses, or interpretation of data; in the writing of the manuscript, and in the decision to publish the results.

Appendix A

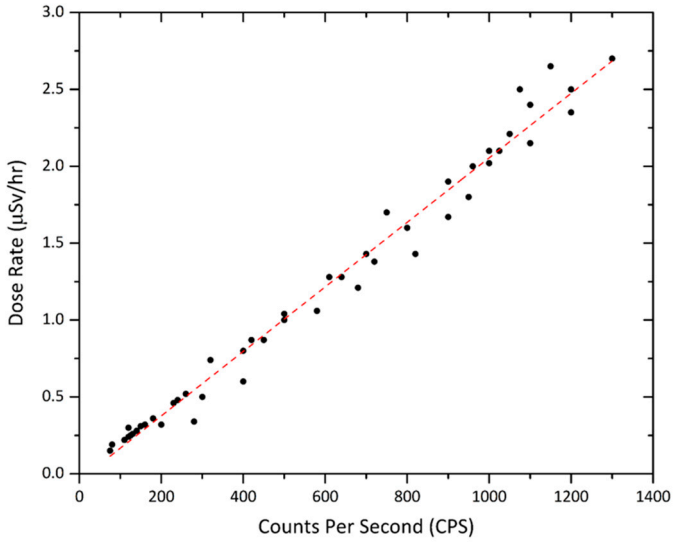

Figure A1. Linear calibration fit between RADEX™ dose-meter (µSv/h) and the Kromek GR1™ system (CPS) deployed on the UAV for a range of isotopes.

References

1. UK National Audit Office. *Nuclear Decomissioning Authority—Progress on the Sellafield Site: An Update*; NAO: Sellafield, UK, 2015.
2. Schwarz, G.F.; Rybach, L.; Barlocher, C.K.; Klingele, E.E. Development and calibration of an airborne radiometric measuring system. *Int. At. Energy Agency* **1995**, *27*, 25–34.
3. Sanderson, D.C.W.; Allyson, J.D.; Tyler, A.N.; Scott, E.M. Environmental applications of airborne gamma spectrometry. *Int. At. Energy Agency* **1995**, *27*, 71–91.
4. Okuyama, S.; Torii, T.; Suzuki, A.; Shibuya, M.; Miyazaki, N. A remote radiation monitoring system using an autonomous unmanned helicopter for nuclear emergencies. *J. Nucl. Sci. Technol.* **2008**, *45*, 414–416. [CrossRef]
5. Mellander, H. The role of mobile gamma spectrometry in the Swedish emergency response programme for nuclear accidents—Experience and future plans. *Int. At. Energy Agency* **1995**, *27*, 187–195.
6. Beamish, D. Environmental radioactivity in the UK: The airborne geophysical view of dose rate estimates. *J. Environ. Radioact.* **2014**, *138*, 249–263. [CrossRef] [PubMed]
7. Sanada, Y.; Kondo, A.; Sugita, T.; Torii, T. Distribution of radioactive cesium measured by aerial radiation monitoring. *Hoshasen* **2012**, *38*, 137–140.
8. Sanada, Y.; Kondo, A.; Sugita, T.; Nishizawa, Y.; Youichi, Y.; Kazutaka, I.; Yasunori, S.; Torii, T. Radiation monitoring using an unmanned helicopter in the evacuation zone around the Fukushima Daiichi nuclear power plant. *Explor. Geophys.* **2014**, *45*, 3–7. [CrossRef]
9. MacFarlane, J.W.; Payton, O.D.; Keatley, A.C.; Scott, G.P.T.; Pullin, H.; Crane, R.A.; Smilion, M.; Popescu, I.; Curlea, V.; Scott, T.B. Lightweight aerial vehicles for monitoring, assessment and mapping of radiation anomalies. *J. Environ. Radioact.* **2014**, *136*, 127–130. [CrossRef] [PubMed]
10. Martin, P.G.; Payton, O.D.; Fardoulis, J.S.; Richards, D.A.; Yamashiki, Y.; Scott, T.B. Low altitude unmanned aerial vehicle for characterising remediation effectiveness following the FDNPP accident. *J. Environ. Radioact.* **2016**, *151*, 58–63. [CrossRef] [PubMed]
11. Martin, P.G.; Payton, O.D.; Fardoulis, J.S.; Richards, D.A.; Scott, T.B. The use of unmanned aerial systems for the mapping of legacy uranium mines. *J. Environ. Radioact.* **2015**, *143*, 135–140. [CrossRef] [PubMed]
12. ArduCopter APM Copter. Available online: http://www.arducopter.co.uk/ (accessed on 1 November 2016).
13. Kromek Group PLC GR1 Spec Sheet. Revision 10. Available online: http://www.kromek.com/products_gr1spectrometer.asp (accessed on 23 June 2015).
14. AR2500 Acuity^{TM} Acuity AR2500 Specification. Available online: http://www.acuitylaser.com (accessed on 3 June 2015).
15. Hubbell, J.H.; Seltzer, S.M. *Tables of X-ray Mass Attenuation Coefficients and Mass Energy-Absorption Coefficients*; Version 1; National Institute of Standards and Technology: Gaithersburg, MD, USA, 2004.
16. CRC Press. *CRC Handbook of Chemistry and Physics—Table of Isotopes*, 96th ed.; Haynes, W.M., Ed.; CRC Press: Boca Raton, FL, USA, 2015.
17. Civil Aviation Authority Small Unmanned Aircraft—Specific Regulations about Small Drones. Available online: https://www.caa.co.uk/Commercial-industry/Aircraft/Unmanned-aircraft/Small-unmanned-aircraft/ (accessed on 1 November 2016).